Chinese Chemical Letters 34 (2023) 107668

Contents lists available at ScienceDirect

Chinese Chemical Letters

journal homepage: www.elsevier.com/locate/cclet

Investigation into the structures and physicochemical properties of multi-component crystals of voriconazole

Hong-Mei Yu[a], Bao-Xi Zhang[a], Wen-Hui Xing[a], Mei-Ju Liu[a], Feng-Feng Wang[b], Ning-Bo Gong[a,*], Li Zhang[a,*], Yang Lu[a,*], Guan-Hua Du[c]

[a] *Beijing Key Laboratory of Polymorphic Drugs, Institute of Materia Medica, Chinese Academy of Medical Sciences and Peking Union Medical College, Beijing 100050, China*
[b] *National Institutes for Food and Drug Control, Beijing 102629, China*
[c] *Beijing City Key Laboratory of Drug Target Identification and Drug Screening, Institute of Materia Medica, Chinese Academy of Medical Sciences and Peking Union Medical College, Beijing 100050, China*

ARTICLE INFO

Article history:
Received 19 May 2022
Revised 12 June 2022
Accepted 6 July 2022
Available online 14 July 2022

Keywords:
Multi-component crystal
Voriconazole
Solubility
Dissolution
Stability

ABSTRACT

Voriconazole (VZL) is a second-generation and broad-spectrum triazole against fungal infections. Being a BCS (biopharmaceutics classification system) class II compound, the poor aqueous solubility has limited its bioavailability and clinical efficacy. Aims to overcome this disadvantage, a cocrystallization strategy based on crystal engineering principles has resulted in five new multi-component crystals of VZL with maleic acid, L-tartaric, protocatechuic, gallic, and 3,5-dinitrobenzoic acids. Structure analysis revealed that the hydroxyl/carboxylic acid···triazole N_3 hydrogen bonding interaction appears as a main supramolecular heterosynthon in the VZL multi-component crystals with organic acids. And VZL molecule has a flexible conformation in each of the five multi-component structures. The newly synthesized multi-component crystals showed impressive solubility improvement compared to that of the raw material of VZL. Molecular electrostatic potential surfaces (MEPS) analysis based on density functional (DFT) calculations revealed that hydrogen bond interactions in cocrystals mainly involved pairwise interactions in the global maxima and minima sites, but this rule is not always followed. This study indicates the potential of cocrystals to improve the solubility and dissolution rate of VZL

It is generally known that the solid phase forms of APIs display variability, including polymorphs, salts, cocrystals, hydrates, and solvates [1]. During the past few years, supramolecular synthons have been employed to prepare pharmaceutical cocrystals with optimized physicochemical properties between active pharmaceutical ingredients (APIs) and organic formers [2]. Cocrystals and salts both are multi-component crystals. Cocrystals consist of two or more neutral compounds held together in a specific stoichiometry through hydrogen bonds, whereas, proton transfer occurs in salts [3]. Pharmaceutical cocrystallization offers the potential of modifying the physicochemical properties of drugs, thus potentially rendering the compound bioavailable without alternating their inherent pharmacological properties. Improvements in solubility, dissolution rate, stability, hygroscopicity, and compressibility have been well documented [4–9]. Besides, cocrystals have been shown to offer efficient options in the pharmaceutical industry for intellectual property protection and extension [10].

Currently, ketoconazole, fluconazole, and itraconazole are commonly used antifungal azoles [11]. In the past decade, a new generation of triazole agents has continuously been in development. Voriconazole ((2*R*,3*S*)-2-(2,4-difluorophenyl)-3-(5-fluoropyrimidin-4-yl)-1-(1*H*-1,2,4-triazol-1-yl)butan-2-ol, $C_{16}H_{14}F_3N_5O$, VZL, Scheme 1), is the first agent to receive approval from the US Food and Drug Administration (FDA), which is a second-generation triazole antifungal drug administered intravenously or in oral dosage formulation [12]. Derived from fluconazole, VZL shows broad-spectrum antifungal activity against a wide variety of yeasts and molds, especially against acute invasive Aspergillus [13], invasive Candida [14], and Fusarium [15], compared with older triazoles. VZL has shown good therapeutic effects in the treatment of invasive pulmonary fungal infections [16–18], and chronic obstructive pulmonary disease with aspergillosis [19,20]. The action mechanism of VZL [21], involves the inhibition of cytochrome CYP 450-dependent 14a-lanosterol demethylation, which is a key step in fungal cell membrane ergosterol synthesis. This inhibition leads

* Corresponding authors.
E-mail addresses: gnb@imm.ac.cn (N.-B. Gong), zhangl@imm.ac.cn (L. Zhang), luy@imm.ac.cn (Y. Lu).

https://doi.org/10.1016/j.cclet.2022.07.011
1001-8417/

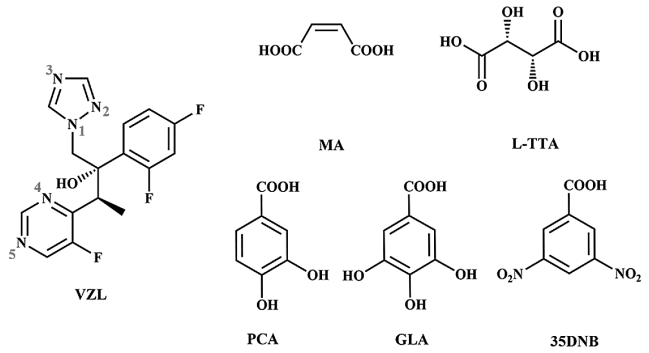

Scheme 1. Chemical structure of voriconazole and the organic acid coformers (CCFs).

to depletion of ergosterol and accumulation of 14-methyl sterols such as lanosterol, affecting fungal cell membrane lipid formation.

The very low aqueous solubility of VZL (0.71 mg/mL) [22] represents a major disadvantage for its efficacy as an oral dosage form. Literature shows that treatment with VZL does carry the risk of toxicity. Reversible disturbance of vision (photopsia) [23], skin rash [24], and abnormal liver function were most frequent [25]. Given its broad and unique spectrum of activity, there is a need to conduct in-depth research to develop novel solid forms of VZL with better solubility, dissolution, stability, and properties suitable for pharmaceutical processing. Thus, the dose of VZL could be reduced and hence less toxic. The crystal engineering technique has been applied to address the solubility issue of VZL. To date, a set of VZL salts (nitric acid, hydrochloric acid, oxalic acid) and cocrystals (fumaric acid, 4-hydroxybenzoic acid, and 4-aminobenzoic acid, *m*-nitrobenzoic acid) have been developed [22,26], which have been prepared to increase the solubility and dissolution rate of VZL.

In this work, all five novel multi-component solid forms of VZL were prepared by solvent evaporation technique as well as liquid-assisted grinding method. Then, their inter- or intramolecular interactions were analyzed carefully for a better understanding of the supramolecular synthons. The nature of the above complexes has been ambiguously confirmed based on the geometry of the carboxyl group and the acid proton location. Furthermore, single crystal X-ray diffraction (SCXRD) analysis revealed that the synthesized multi-component crystals were formed through a robust hydroxyl/carboxyl hydrogen···triazole N hydrogen bonding involving -OH/-COOH of coformers (CCFs) and triazole group of the VZL molecule. To facilitate the design of multi-component crystals, it is critical to extend our understanding of the self-assembly principle through further crystallographic studies at the synthon level. It is pointed out that the most positive and negative values of the electrostatic surface potential (ESP) show a promising advantage in identifying the sites of non-covalent interactions [27,28]. The maximum and minimum extreme values of VZL and CCFs were calculated based on the MEPS. To understand the formation mechanisms and to investigate the properties of the multi-component crystals, further comprehensive solid-state characterizations including powder X-ray diffraction (PXRD), differential scanning calorimetry (DSC), thermogravimetric analysis (TGA), and Fourier transform infrared (FT-IR) spectroscopy were carried out. Systematic solubility and dissolution experiments of the obtained multi-component crystals in pure water were also performed, and an approximately 2.7-fold solubility improvement was achieved at 8 h in pure water. Improved solubility could lower the doses of the active drugs in use, thereby reducing the incidence and severity of side effects potentially. We hope that our work will contribute to deepening the understanding of supramolecular synthons and thus improve the efficiency of cocrystal design.

VZL raw material was purchased from Wuhan Yinhe Chemical Co., Ltd. (Hubei, China). Organic acids: MA (98%), L-TTA (98%), PCA (99%), GLA (99%), and 35DNB (purity > 97%) were purchased from Beijing Chemical Reagent Co. (Beijing, China). All analytical grade solvents were purchased from Sigma Aldrich (St. Louis, MO, USA) and were used without further purification.

The solvent-assisted grinding method was applied for the preparation of VZL multi-component crystals. Slow evaporation was used to harvest the single crystals for SCXRD analysis. The detailed preparation processes were provided in the supporting information.

SCXRD data were collected on a Rigaku Micromax 002+ diffractometer (USA) equipped with a CCD detector and a graphite monochromator (Cu *Ka* radiation, $\lambda = 1.54184$ Å). Data collections were performed at 295 K using a CrysAlisPro system attached to the diffractometer. The crystal structures were solved by SHELXT-2018 [29] (Sheldrick, 2016) using a direct method, and refined by the full-matrix least-squares method on F^2 using the SHELXL program.

Theoretical MEPS calculation of the VZL and CCFs (MA, TTA, PCA, GLA, 35DNB) was implemented using the DFT method at b3lyp level with 6-311g(d) basis set [30,31]. The Gaussian 16 package was utilized for all calculations [32]. The Multiwfn 3.8 software and the VMD software were employed to evaluate the topological properties of all compounds [33–35]. The MEPS values were used to determine the potential surface hydrogen bonding interaction sites which were the main driving forces for cocrystal formation [36].

PXRD patterns were collected on a Rigaku X-ray powder diffractometer (D/max-2550, Japan) with Cu *Kα* radiation ($\lambda = 1.54178$ Å), which was recorded from 3°-40° in 2θ with a scan rate of 8°/min and a step size of 0.02°. The tube voltage and amperage were set to 40 kV and 150 mA, respectively. The program Mercury 3.0 was employed for the simulation of theoretical PXRD patterns calculated from the SCXRD data.

DSC spectra were recorded using a differential scanning calorimeter (Mettler Toledo, Greifensee, Switzerland). The samples (about 5-6 mg) were accurately weighed and placed in an aluminum pan pricked with a pinhole, and the analysis was conducted at a scan rate of 10 °C/min.

TG measurements were carried out using a TGA/DSC STARe system (Mettler Toledo, Greifensee, Switzerland). The accurately weighed powder samples were heated from 30 °C to 500 °C in aluminum oxide cells at a heating rate of 10 °C/min under a nitrogen gas flow of 50 mL/min. Analyses of the traces obtained from the DSC and TGA measurements were carried out using the STARe software.

The FT-IR spectrometry was recorded in the 650-4000 cm^{-1} spectral domain at a resolution of 4 cm^{-1} using a PerkinElmer Spectrµm 400 FT-IR instrument under ambient conditions.

The high performance liquid chromatography (HPLC) method was carried out on an Agilent 1260 HPLC/UV (Agilent Technologies, USA) system. The HPLC conditions were as follows: a SilGreen C_{18} (250 mm × 4.6 mm, 5 µm) column; the mobile phase, acetonitrile, and 0.02 mol/L ammonium acetate water solution (45:55, v:v); flow rate, 1.0 mL/min; column temperature, 30±0.2 °C; injection volume, 5 µL; detection wavelength, 254 nm.

Equilibrium solubility was determined on a ZHWY-103D thermostatic shaker-incubator (Shanghai Zhicheng Analytical Instrument Manufacturing Co., Ltd.) using the shake-flask method. To obtain the equilibrium solubility, excess solid powders of VZL and its multi-component crystals were added to glass vials containing 3 mL ultrapure water. The solutions were agitated continuously at a rate of 160 strokes/min for 48 h, with the temperature kept at 37±0.5 °C. The suspension was filtered through a 0.22 µm nylon filter, and appropriate dilution was applied to the filtrate followed

Table 1
Crystallographic information and structure refinement parameters for VZL multi-component crystals.

Parameter	VZL-MA	VZL-TTA	VZL-PCA-H_2O	VZL-GLA	VZL-35DNB
formula	$C_{20}H_{18}F_3N_5O_5$	$C_{20}H_{20}F_3N_5O_7$	$C_{23}H_{20.50}F_3N_5O_{5.25}$	$C_{23}H_{20}F_3N_5O_6$	$C_{23}H_{18}F_3N_7O_7$
Formula weight	465.39	449.41	507.94	519.44	561.44
Crystal size (mm)	$0.02 \times 0.03 \times 0.26$	$0.06 \times 0.35 \times 0.42$	$0.35 \times 0.51 \times 0.56$	$0.05 \times 0.26 \times 0.51$	$0.11 \times 0.25 \times 0.29$
Description	needle	plate	block	plate	prism
Crystal system	monoclinic	monoclinic	monoclinic	monoclinic	orthorhombic
Space group	$P\,2_1$	$P\,2_1$	$C\,2$	$C\,2$	$P2_12_12_1$
a (Å)	9.588(1)	8.008(1)	23.283(1)	16.076(1)	5.652(1)
b (Å)	5.687(1)	34.935(2)	8.031(1)	7.154(1)	14.650(1)
c (Å)	18.883(1)	8.047(1)	12.849(1)	21.005(1)	29.947(1)
α (°)	90	90	90	90	90
β (°)	93.16(1)	101.61(1)	98.29(1)	105.62(1)	90
γ (°)	90	90	90	90	90
Volume (Å^3)	1028.04(4)	2205.27(17)	2377.59(2)	2326.66(6)	2480.05(5)
Density (g/cm^3)	1.503	1.504	1.419	1.483	1.504
Independent reflections	2993	7601	3954	4238	4756
Reflections with $I > 2\sigma(I)$	2675	6564	3942	4166	4634
R_{int}	0.048	0.052	0.024	0.037	0.033
final R, $wR(F^2)$ value [$I > 2\sigma(I)$]	0.035, 0.089	0.061, 0.163	0.040, 0.105	0.038, 0.107	0.038, 0.110
GOF	1.071	1.061	1.085	1.032	1.080
CCDC number	2167826	2167823	2167827	2167824	2167825

by the analysis of VZL concentrations using the aforementioned HPLC method. Each experiment was repeated in triplicate. Residual solids after equilibrium experiment were checked by PXRD.

The powder dissolution profiles of VZL and its multi-components were performed by using a RC12AD dissolution apparatus (Tianjin TIANDA TIANFA-pharmaceutical testing instrument manufacturer), equipped with an autosampler RZQ-12D Dissolution Sampling Station with the following parameters: (1) Medium: ultrapure water, 450 mL; (2) Apparatus (basket): rotation speed of 100 rpm; (3) Times: 3, 6, 9, 12, 15, 30, 60, 120, 180, 240, 360 and 480 min; (4) Temperature: 37±0.2 °C. Aliquots were withdrawn at regular intervals and filtered through a 0.22 μm nylon filter, and then the concentrations of VZL were assayed by the HPLC method. Each experiment was repeated in triplicate. Residual solids were collected after the dissolution test and characterized by PXRD.

The stability properties of the multi-component crystals were evaluated in a drug stability test instrument (SHH-150SD). Powder samples were stored under three accelerated storage conditions, high temperature (60±1 °C), high humidity (90% ± 5%, 25 °C), and light (4500 ± 500 lx, 25 °C) [36], respectively. The samples were taken out at time intervals of 5 and 10 days, and the phase stability of samples was measured by comparing the PXRD patterns of initial and final samples. In this work, a long-term stability study was also conducted (25±5 °C and 60%±5% RH) for 6 months.

The design of multi-component crystals may be achieved with the identification and utilization of homo- and heterosynthon hydrogen-bonding rules [37–39]. When screening for cocrystals, it is essential to consider the functional groups present in the molecule and to select those CCFs with complementary groups. The presence of triazole and pyrimidine rings in VZL enables the formation of several possible supramolecular synthons with complementary functional groups (-OH, -COOH, -NH_2) for the synthesis of multi-component systems. In our search for new solid forms of VZL, the acid···$N_{heterocyclic}$ supramolecular synthon was targeted by crystallizing with CCFs containing acid -OH, -COOH functionalities. Therefore, a series of aliphatic dicarboxylic acids and aromatic acids were chosen to conduct the multi-component crystal screening work. Four cocrystals of VZL were produced, while maleic acid yielded a molecular salt in the cocrystallization. The new crystal structures of VZL-MA (1:1) salt, cocrystals of VZL-PCA-H_2O (1:1:0.25), VZL-TTA (1:1), VZL-GLA (1:1), and VZL-35DNB (1:1) are discussed in this paper. By applying the solvent-assisted grinding method, cocrystal screening of VZL in combination with acids (malonic, glutaric, citric, malic, salicylic) led to clay materials, while with ferulic, benzoic, caffeic, and phthalic acids, the resulting PXRD patterns tended out to be the physical mixture of VZL and the corresponding CCF. A summary of the crystallographic information and structure refinement parameters of the new multi-components are provided in Table 1. Hydrogen bond geometrical parameters of crystal structures are provided in Table S1 (Supporting information).

VZL-MA (1:1, Fig. 1a) crystallizes in the monoclinic crystal system in a stoichiometric ratio of 1:1, space group $P\,2_1$ ($Z=2$), and the asymmetric unit consists of one VZL cation with protonated triazole N_3 atom and one MA anion ($Z'=1$). In $(VZL\text{-}H)^+ \cdot (MA)^-$, the acidic proton was localized on a difference Fourier map near the triazole nitrogen atom. The proton transfer from carboxyl of MA to triazole N_3 atom of VZL confirms its ionic nature. The distances of C=O and C-OH within the carboxyl group in MA differ by less than 0.02 Å (0.002 Å), which also proved that the VZL-MA should be considered as a salt. There is a common intramolecular $O_1\text{-}H_1\cdots N_4$ hydrogen bond between the pyrimidine N_4 atom and hydroxyl group within VZL molecule. For MA, an intramolecular $O_3\text{-}H_{3a}\cdots O_4$ hydrogen bond is also observed. The planar MA anions and VZL cations link alternately to form a motif stabilized by $N_3\text{-}H_3{}^+\cdots O_5{}^-$ salt bond. More specifically, the crystal structures of the VZL-MA salt display a "chevron-like" arrangement of the MA anions scattered in the voids enclosed by VZL cations. The chains align parallel to the c-axis and form a "wavy" zig-zag sheet packing arrangement sustained by the $C_{10}\text{-}H_{10}\cdots N_5$ forces.

VZL-TTA (1:1, Fig. 1b) cocrystal crystallizes in the monoclinic crystal system, space group $P\,2_1$ ($Z=4$) with two VZL molecules (suffix with A and B) and two TTA (suffix with A and B) molecules in the asymmetric unit ($Z'=2$, Fig. 1b). Intramolecular $O_{1A}\text{-}H_{1A}\cdots N_{4A}/O_{1B}\text{-}H_{1B}\cdots N_{4B}$ hydrogen bonds exist within each VZL molecule. VZL interacts with TTA through $O_{3A}\text{-}H_{3A}\cdots N_{2A}$, $O_{4A}\text{-}H_{4Aa}\cdots N_{3A}$, $O_{3B}\text{-}H_{3B}\cdots N_{2B}$, $O_{4B}\text{-}H_{4Ba}\cdots N_{3B}$ hydrogen bonds. TTA molecules have interacted through $O_{6A}\text{-}H_{6A}\cdots O_{5B}$, $O_{6B}\text{-}H_{6B}\cdots O_{5A}$ hydrogen bonds with each other to form a two-dimensional (2D) net-like structure, and are sandwiched between the double layers of VZL, viewed along the crystallographic a-axis.

VZL-PCA-H_2O (1:1:0.25, Fig. 1c) cocrystal crystallizes in the monoclinic space group $P\,2_1$ ($Z=4$) with one VZL, one PCA, and a quarter water molecule in the asymmetric unit ($Z'=1$). Hydrogen bonding $O_5\text{-}H_5\cdots N_3$ existed between the triazolyl group of VZL and the carboxyl (-COOH) group in PCA. The annular arrangement of VZL and PCA molecules is further stabilized by O-H···O interactions between the hydroxyl group -OH and the water molecule.

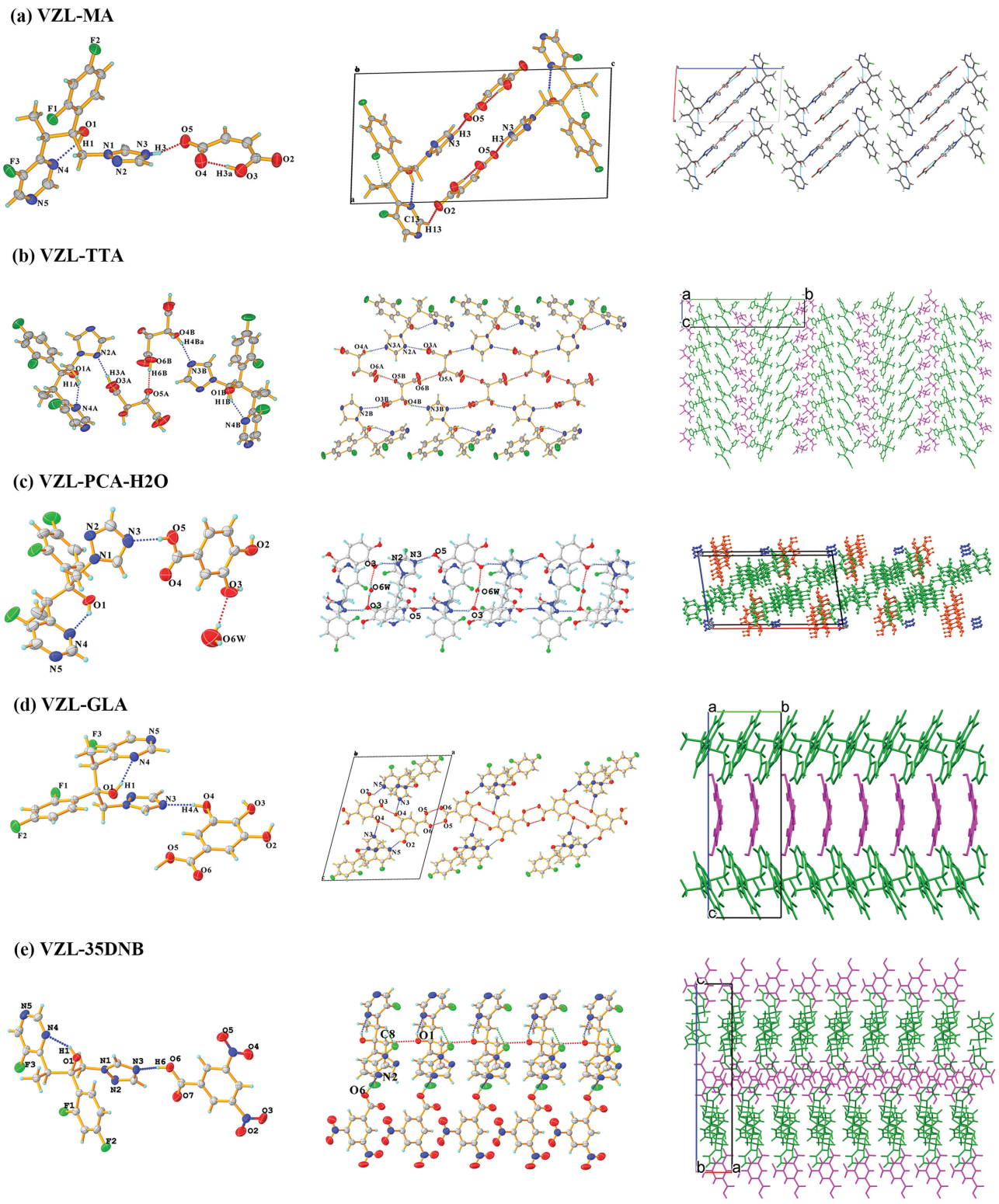

Fig. 1. (a-e) The asymmetric units (left), hydrogen bond motifs (medium), and packing of the crystal structures (right).

VZL-GLA (1:1, Fig. 1d) crystallizes in the monoclinic space group *C* 2 (*Z*=4), with one VZL and one GLA molecule in the asymmetric unit ($Z' = 1$). All of the VZL molecules also form O_1-H_1···N_4 intramolecular hydrogen bonds. O_4-H_4···N_3 hydrogen-bonding interaction involving the free hydroxyl group of GLA and triazolyl N_3 atom appears as a main supramolecular heterosynthon. Noticeably, the dimeric units interacted *via* an O_4-H_4···O_3 homosynthon between the GLA hydroxyl groups to generate a centrosymmetric tetrameric motif, and further extended through O_5-H_5···O_6 homosynthon between the carboxylic acid group of GLA. GLA molecules are sandwiched between the double layers of VZL, and extended along crystallographic b-axis. These tetrameric motifs are held together into a 2D layered architecture throughout the crystal structure *via* weak interactions.

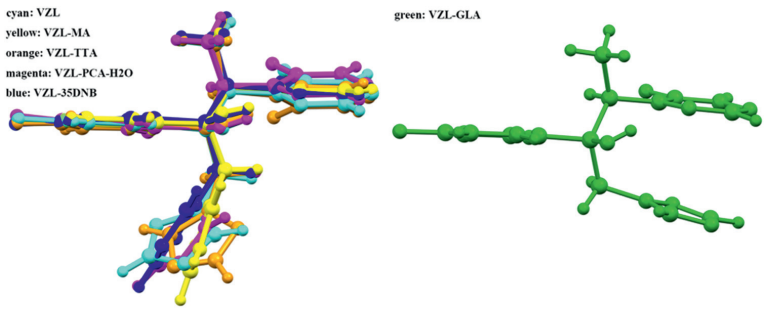

Fig. 2. Overlay of VZL conformations in the VZL pure drug and its multi-component crystals. Triazole and pyrimidine rings are *anti* in the VZL-MA salt, VZL-TTA, VZL-PCA-H_2O, VZL-35DNB cocrystals, while they are *syn* in the VZL-GLA cocrystal.

VZL-35DNB (1:1, Fig. 1e) crystallizes in the orthorhombic crystal system, space group $P\,2_12_12_1$ ($Z=4$). The asymmetric unit consists of one VZL molecule and one 35DNB molecule ($Z'=1$). There is a common intramolecular O_1-$H_1\cdots N_4$ hydrogen bond within VZL between the pyrimidine N_1 atom and hydroxyl group. The VZL and 35DNB molecules form a pair sustained by the (carboxyl) O_6-$H_6\cdots N_3$ (triazolyl) hydrogen bond. The pairs interact with each through the weak C_8-$H_8\cdots O_1$ hydrogen bond, forming a 1D molecular chain propagating along a-axis, and further fabricated into a 3D sandwich-like structure *via* weak interactions.

Structural analysis revealed that the primary supramolecular interactions involved mainly but not limited to -O-H···N, -C=O-O-H···N and -N-H···N hydrogen bonds, involving predominantly -NH_2, -OH and -COOH donor groups of CCFs, and triazole or pyrimidine N atoms of VZL in all of the reported and synthesized multi-component crystals. Phenolic hydroxyl···triazole N_3 appears as the primary supramolecular heterosynthon in VZL cocrystals, corresponding to the report that "The proton-donating ability of the phenolic hydroxyl group is equivalent or slightly higher than that of the carboxylic acid group" [40]. The results reinforce our interaction search with aliphatic and aromatic carboxylic acids and further aid in CCF selections for nitrogen heterocyclic compounds.

Literature reported by Palash Sanphui has seen the torsional flexibility in cocrystals and salts of VZL [26]. The orientation of the triazole ring of VZL in the cocrystals with fumaric, *p*-hydroxybenzoic, *p*-aminobenzoic, 3-nitrobenzoic acids as CCFs is syn with respect to the pyrimidine moiety of VZL, while in the anti position in the salts with hydrochloric, oxalic and nitric acids. In the current work, flexible orientations are also found to be adopted by triazole and pyrimidine rings of VZL. Structure overlay of VZL conformations in the multi-component crystal structures has shown that triazole and pyrimidine rings are anti in the VZL-MA salt, VZL-TTA, VZL-PCA-H_2O, VZL-35DNB cocrystals, but they are syn in the VZL-GLA cocrystal (Fig. 2). Generally, the *cis* or *trans* conformation has little to do with the formation of salt or cocrystal. In the cocrystal structures of Entacapone [41], different conformations and orientations were also observed due to rotation about single bonds. Hydrogen bonding interactions with CCF could change the conformation of the drug due to stronger hydrogen bonding and different molecular packing requirements. Conversely, conformational flexibility of API enables more options of CCFs to synthesize cocrystals.

The positive or negative extrema based on the MEPS can be able to visualize the potential donor and acceptor sites clearly and is useful for predicting cocrystal formation. The strongest hydrogen bond donor and acceptor site in a solid are likely to be paired in the cocrystallization process according to Etter's rule [37]. Fig. 3 presents the ESPs of VZL and CCFs (MA, TTA, PCA, GLA and 35DNB) marked with maxima and minima values (unit: kcal/mol). The minima and maxima of MESP are depicted as cyan and orange spheres and labeled by dark blue and red text, respectively. From the MESPs map of VZL and selected CCFs, VZL could act as a hydrogen bond acceptor in the cocrystallization owing to the negative potential parts (ESP of triazole $N_3=-43.58$, triazole $N_2=-33.51$, pyrimidine $N_5=-20.49$ kcal/mol). MA (ESP of -COOH = +68.06 kcal/mol), TTA (ESP of -OH = +31.11 kcal/mol, -COOH = +53.46/+62.04 kcal/mol), PCA (ESP of -OH = +42.66/+59.76 kcal/mol, -COOH = +51.63 kcal/mol), GLA (ESP of -O_4H = +64.01 kcal/mol) and 35DNB (ESP of -COOH = +68.77 kcal/mol) could act as good proton donors. The dominating interactions that drove the formation of VZL-MA salt and cocrystals with GLA, 35DNB follow Etter's rule, where the largest positive potential sites of CCFs and the largest negative ones are paired. In addition, the formation of the VZL-PCA-H_2O involves

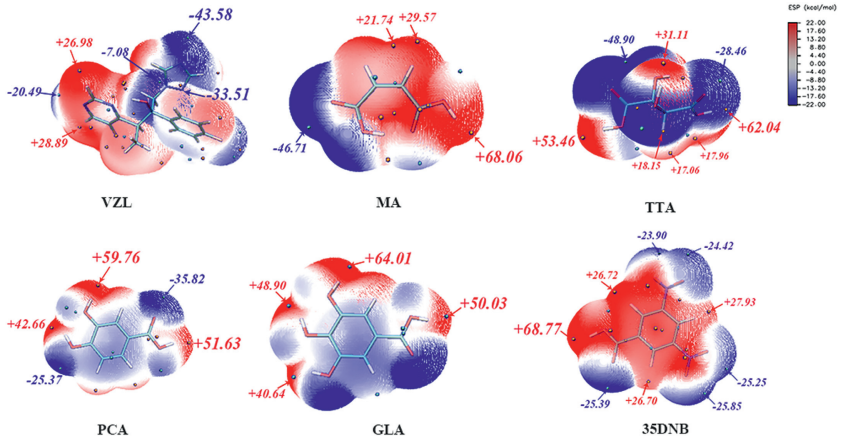

Fig. 3. The positive and negative extreme values (kcal/mol) from MEPS of discrete VZL, MA, TTA, PCA, GLA and 35DNB.

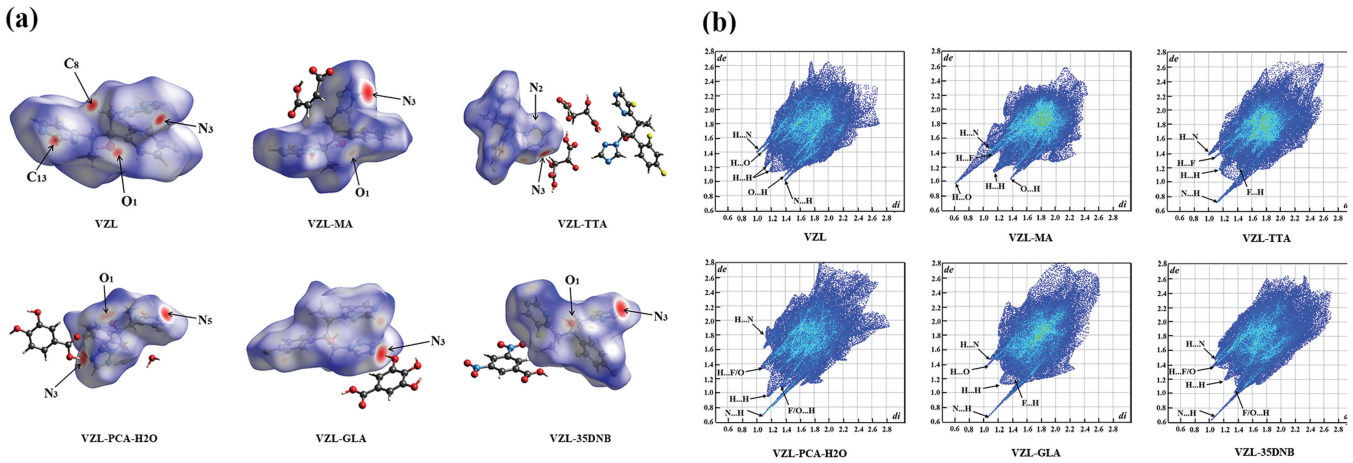

Fig. 4. (a) The Hirshfeld surfaces map for the VZL pure drug and its multi-component crystals. (b) The 2D fingerprints of intermolecular interactions in VZL and its multi-component crystals.

the second largest positive potential site of PCA and the largest negative potential site of VZL. It seems that Etter's rule does not exactly be followed in the VZL-TTA molecule, as there are two molecules each of VZL and TTA in the asymmetric unit.

Molecular Hirshfeld surfaces of VZL multi-component crystals were analyzed using the Crystal Explorer 3.1 program [42] and were presented in Fig. 4a. The red and blue regions on the visualized surface represent the strong and weak contacts, respectively. Fig. 4b shows the 2D fingerprints of intermolecular interactions in the VZL multi-component crystals, which reflects the interaction force between molecules within the structure and the contribution percentage of each. triazole N_3 atom and pyrimidine N_5 atom act as main hydrogen bond acceptors. The 2D fingerprint plots showed that intermolecular N···H, F···H and O···H intermolecular interactions are dominant and match the Hirshfeld surfaces. Among the five cocrystals of VZL, the N atom on the triazole ring mainly acts as a hydrogen bond acceptor to participate in the formation of hydrogen bonds, so the N···H force is stronger than the H···N force, while H···N is stronger than N···H interactions as the H atom was transferred to the triazolyl group in the VZL-MA salt. The results agree with SCXRD data and MEPS calculations performed.

PXRD allows an attractive avenue to identify new solid forms from a physical mixture of API and CCF. If there is appearance of new peaks or disappearance of some characteristic peaks from the individual components in the PXRD pattern, a new phase can be assumed to form [43]. PXRD patterns of VZL, its multi-components, simulated ones, and five CCFs have been exhibited in Fig. 5a. It can be found that the patterns of the products are distinct from either that of VZL or those of the corresponding CCFs. Besides, peaks displayed in the experimental patterns of the bulk powder are closely matched with those calculated from the SCXRD data, indicating consistent and satisfactory pure phases.

The DSC analysis could be utilized to identify the formation of novel solid forms and to characterize the thermal stability of the solid phases [44]. The melting temperature of VZL-TTA (139.5 °C), VZL-PCA-H_2O (119.4, 142.3 °C) and VZL-GLA (142.3 °C) are intermediate compared to that of the VZL drug (133.3 °C) and corresponding CCFs, whereas VZL-MA (89.1 °C) salt and VZL-35DNB (114.3 °C) cocrystal exhibit lower melting point than either of the starting components (Fig. 5b). Endotherm peak at 119.4 °C is ascribed to the one-quarter crystal water molecule in the VZL-PCA-H_2O. Further, all of the multi-component crystals exhibited a sharp endotherm in the thermograms, manifesting the high purity of the synthesized complexes. The TG profiles of VZL, and its multi-component crystals have been deposited in Fig. S1 (Supporting information).

Table 2
Experimental Solubility of VZL and multi-component crystals in ultrapure water at 37.0 °C.

Crystal	Concentration (μg/mL)	
	Solubility after 8 h powder dissolution test	Equilibrium solubility after 48 h shaking
VZL	250.20±23.52	835.26±155.00
VZL-MA	688.24±27.21	1285.40±163.37
VZL-TTA	685.88±21.24	944.54±12.14
VZL-PCA-H_2O	665.70±40.85	911.20±147.00
VZL-GLA	661.81±39.61	1070.29±45.69
VZL-35DNB	677.30±18.50	985.23±58.61

Possessing the ability to featuring new absorption bands, shifting, broadening, and disapearances of band(s), FT-IR spectroscopy could be utilized as a complementary tool to PXRD to evidence the non-covalent interactions within the crystals [45]. The most characteristic shifts of vibration bands of VZL multi-component crystals are observed at 1600-1750 cm^{-1}, corresponding to the stretching vibration of the carboxyl group in CCFs, suggesting the structural involvement of CCFs (Table S2 in Supporting information).

Equilibrium solubility and apparent powder dissolution properties of VZL salt and cocrystals were performed in ultrapure water to evaluate the solid form. Only the solubility of VZL was measured for each compound and the concentration of VZL in saturated solution is referred to as the equilibrium solubility of API. The solubility results were displayed in Table 2. The PXRD patterns of residual solids after the equilibrium experiment were provided in Fig. S2 (Supporting information). VZL raw material remained in its initial phase during the equilibrium and apparent dissolution test at pure water. VZL-MA and VZL-TTA totally dissociated into VZL. VZL-PCA-H_2O and VZL-GLA partially dissociated into VZL, evidenced by the diffraction peaks of VZL and corresponding cocrystals, while VZL-35DNB remained its cocrystal phase after equilibrium solubility experiment.

An enhancement in dissolution rate plays an important role in the release of a drug, thus impacting their effectiveness, which is advantageous for the development of solid-state drugs [46,47]. The dissolution behaviors of VZL, and five multi-component crystals were investigated in ultrapure water (Fig. 6). The dissolution rate is significantly improved as compared to VZL pure drug, and the apparent solubility values of VZL-MA, VZL-TTA, VZL-PCA-H_2O, VZL-GLA, and VZL-35DNB are approximately 2.7 times as large as that of VZL at 8 h as revealed by the powder dissolution test

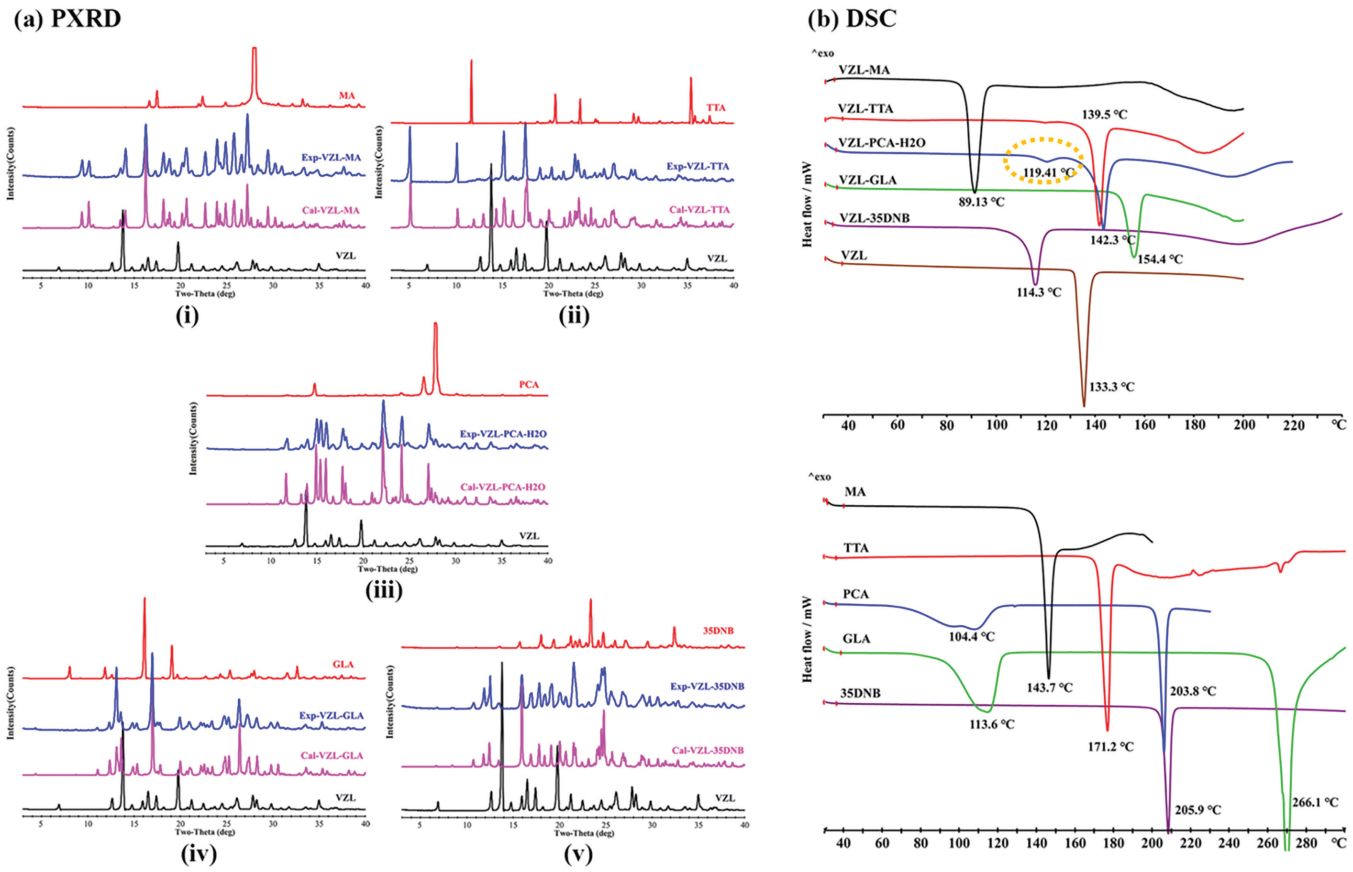

Fig. 5. (a) Powder X-ray diffraction patterns of (i) VZL-MA, (ii) VZL-TTA, (iii) VZL-PCA-H_2O, (iv) VZL-GLA, (v) VZL-35DNB, including the raw materials, and simulated PXRD patterns calculated from SCXRD data. (b) The DSC thermograms of VZL, its multi-component crystals and corresponding CCFs.

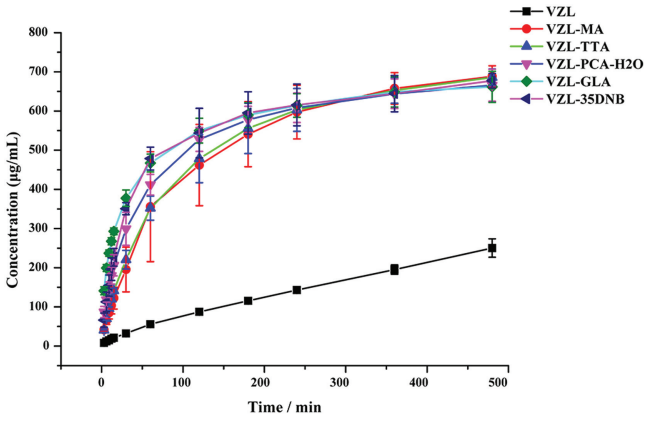

Fig. 6. The dissolution profile of VZL pure base and its multi-component crystals in pure water for 8 h.

(Table 2). These results indicate that the strategy of synthesizing salts and/or cocrystals provides a facile route to enhance the solubility and dissolution rate of APIs. The PXRD patterns of residual solids after the powder dissolution experiment were also evaluated and provided in Fig. S2. VZL-MA, VZL-TTA, VZL-PCA-H_2O and VZL-GLA completely dissociated into VZL, and VZL-35DNB partially converted to VZL after powder dissolution test.

Three possible mechanisms are proposed to explain the solubility enhancement of VZL by cocrystallization. (1) By incorporating a CCF into the crystal lattice, along with rearrangements of crystal packing and spatial structure, increased intermolecular distance, decreased lattice energy, and reduced melting enthalpy of the cocrystal were acquired, thereby the solubility of the cocrystal was improved [48,49]. (2) The CCFs possess higher solubility than API: MA (790 g/L), L-TTA (1390 g/L), PCA (29.4 g/L), GLA (1.5 g/L), and 35DNB (1.3 g/L) at 25 °C. It has been previously reported that the solubility of cocrystal is proportionally related to the solubility of its constituents [48–51]. (3) The dissociation of hydrogen-bonded structures of multi-component crystals of VZL resulted in higher apparent solubility. The disolvation of highly aqueous soluble CCF in water escaping from the crystal lattice resulted in the dissociation of cocrystals and breaks of the packing structure, leaving an "amorphous" structure with loose self-aggregation, increasing the exposure area of VZL and CCF molecules, so that the approach of water molecules is facilitated, thus increasing the solubility of cocrystals. The CCF with higher solubility may dissolve and dissociate more quickly from the corresponding cocrystal, hence leading to poorer solution stability. As far as the literature is concerned, the dissociable cocrystal eventually dissociated into the drug and CCF in solution show higher apparent solubility [51–54].

The evaluation of physicochemical stability is an important step in pharmaceutical development. Throughout the testing period, all samples remained stable, except with only a minor stability issue in VZL-TTA cocrystal after 10 days in high humidity (Fig. S3 in Supporting information). There was an appearance at 2θ values of 6.8 corresponding to the characteristic peak of API, which is the sign of cocrystal dissociation, but other peak positions remained consistent. Besides, all the synthesized multi-component crystals are stable under conditions (25 ± 5 °C and 60% ± 5% RH) for 6 months in the long-term stability study, as no significant change was observed in the PXRD patterns between initial and final samples (Fig. S4 in Supporting information).

In conclusion, being a powerful tool for improving the solubility and dissolution rate of poorly soluble drugs, the crystal engineering technique was employed in this study. The aim was that of discovering biologically acceptable systems with a more favorable solubility profile concerning the VZL pure drug. The rational selection of CCFs possessing favorable functional groups (–OH, –COOH) for cocrystallization has successfully resulted in five new solid forms of antifungal drug VZL. Cocrystal screening based on crystal engineering principles proved to be useful for the fast selection of CCFs that are likely to form a molecular assembly with API. Computational analysis further elaborated on the intensities and sites of hydrogen bond interactions in these multi-component crystals by using the MEPS and Hirshfeld surface analysis. The detailed crystal structure analysis and solid-state characterizations were conducted using various XRD, spectral, and thermal techniques. Besides, a series of experiments on physicochemical properties associated with equilibrium solubility, apparent powder dissolution, and accelerated/long-term stability have been evaluated for the five multi-component crystals in comparison with the pure drug.

Crystal structure analysis revealed that the bold heterosynthons mainly include -O-H···N, -C=O-O-H···N, and -N-H···N hydrogen bonding interactions in all of the newly synthesized and reported multi-component crystals. The crystallography research shows some interesting results distinct from previous reports. Torsion flexibility is observed in the VZL multi-component crystals, and both *cis* or *trans* conformation of triazole and pyrimidine rings can be seen in the VZL cocrystals. Thermal analysis revealed that the melting points of VZL-TTA, VZL-PCA-H_2O, and VZL-GLA cocrystals are higher than that of VZL pure drug. The molecular Hirshfeld surface analysis indicates the dominant participation of N···H, F···H and O···H interactions within the multi-component crystal, thus contributing to the crystal packing and electronic properties.

Notably, all the synthesized multi-component crystals are stable in the long-term stability study under ambient conditions (25±5 °C and 60%±5% RH) for 6 months. Concomitantly, newly multi-component crystals displayed enhanced solubility and dissolution rate, probably owing to a reduction in lattice energy, better hydrophilicity of CCFs, and dissociation of multi-component crystals during the dissolution process. Our work implies a promising advantage of the cocrytallization technique for optimizing the solubility and dissolution rate of APIs.

Declaration of competing interest

The authors declare no potential conflicts of interest.

Acknowledgment

This work was supported by Beijing Natural Science Foundation (No. 7222261), Key R&D Program of Shan Dong Province (No. 2021ZDSYS26), the Fundamental Research Funds for the Central Universities (No. 2021-RW350-001), the Xinjiang Uygur Autonomous Region Innovation Environment Construction Special Fund and Technology Innovation Base Construction Key Laboratory Open Project (No. 2022D04016).

Supplementary materials

Supplementary material associated with this article can be found, in the online version, at doi:10.1016/j.cclet.2022.07.011.

References

[1] M.Y. Gokhale, R.V. Mantri, Dev. Solid Oral Dosage Forms (Second Ed) 6 (2017) 85–112.
[2] K. Nimmy, G. Animesh, Curr. Pharm. Des. 26 (2020) 4858–4882.
[3] O.D. Putra, T. Yoshida, D. Umeda, et al., Cryst. Growth Des. 16 (2016) 5223–5229.
[4] Y. Wicaksono, B. Wisudyaningsih, T.A. Siswoyo, Trop. J. Pharm. Res. 16 (2017) 1497–1502.
[5] V.A. Arsul, R.N. Gopale, S.G. Shep, et al., J. Pharm. Res. 9 (2015) 556–561.
[6] M.D. Perera, A.S. Sinha, C.B. Aakeröy, Can. J. Chem. 98 (2020) 1–7.
[7] D.P. Kale, B. Ugale, C.M. Nagaraja, et al., Mol. Pharmaceutics 16 (2019) 2980–2991.
[8] L. Keshavarz, R.R.E. Steendam, M.A.R. Blijlevens, et al., Cryst. Growth Des. 19 (2019) 4193–4201.
[9] M. Karami-Jafari, L. Padrela, G.M. Walker, et al., Cryst. Growth Des. 18 (2018) 6370–6387.
[10] A. Newman, R. Wenslow, AAPS Open 2 (2016) 2.
[11] H. Friccius, H. Pohla, M. Adibzadeh, et al., Int. J. Immunopharmacol. 14 (1992) 791–799.
[12] H. Elewa, E. El-Mekaty, A. El-Bardissy, et al., Clin. Pharmacokinet. 54 (2015) 1223–1235.
[13] R. Herbrecht, D.W. Denning, T.F. Patterson, et al., N. Engl. J. Med. 347 (2002) 408–415.
[14] M. Hui, M.L. Chin, L.K. Chan, et al., Int. J. Antimicrob. Agents 29 (2007) S561–S562.
[15] C. Sagnelli, L. Fumagalli, A. Prigitano, et al., J. Antimicrob. Chemother. 57 (2006) 796–798.
[16] H. Gao, J.R. Wang, H.J. Li, et al., Chin. J. Nosocomiol. 13 (2014) 291–300.
[17] J.A. Cecil, R.P. Wenzel, Expert Rev. Hematol. 2 (2009) 237–254.
[18] I.F. Kuo, M.H.H. Ensom, Can. J. Hospital Pharm. 62 (2014) 469–482.
[19] G. Cucchetto, A. Cazzadori, M. Conti, et al., Infect 43 (2014) 277–286.
[20] T. Saito, S. Fujiuchi, Y. Tao, Infect. 40 (2012) 661–667.
[21] L.A. Jeu, F.J. Piacenti, A.G. Lyakhovetskiy, Clin. Ther. 25 (2003) 1321–1381.
[22] S.S. Kumar, R. Thakuriaa, A. Nangia, CrystEngComm 16 (2014) 4722–4731.
[23] J. Kinoshita, N. Iwata, M. Ohba, et al., Invest. Ophthalmol. Vis. 52 (2011) 5058–5063.
[24] A. Amanati, P. Badiee, M. Lotfi, et al., Curr. Med. Mycology. 6 (2020) 73–78.
[25] K. Tan, N. Brayshaw, K. Tomaszewski, et al., J. Clin. Pharm. 46 (2013) 235–243.
[26] P. Sanphui, M.K. Mishra, U. Ramamurty, et al., Mol. Pharm. 12 (2015) 889–897.
[27] P. Politzer, J.S. Murray, Cryst. Growth Des. 15 (2015) 3767–3774.
[28] K. Wang, X. Zhao, W.H. Zhu, Cryst. Res. Tech. 54 (2019) 1900171.
[29] G.M. Sheldrick, Acta Crystallogr., Sect. A: Found. Adv. 71 (2015) 3–8.
[30] B. Sezgin, B. Dede, I.K. Atay, et al., Arabian J. Sci. Eng. 46 (2020) 5567–5581.
[31] M.M. Lawal, T. Govender, G.E.M. Maguire, et al., Int. J. Quantum Chem. 118 (2018) e25497.
[32] M.J. Frisch, G.W. Trucks, H.B. Schlegel, et al., Gaussian 16 (2016) rev. A.03; Gaussian, Inc.Wallingford, CT.
[33] T. Lu, F.J. Chen, Comput. Chem. 33 (2012) 580–592.
[34] T. Lu, F.W. Chen, Cryst. Growth Des. 117 (2013) 3100–3108.
[35] W. Humphrey, A. Dalke, K. Schulten, J. Mol. Graphics 14 (1996) 33–38.
[36] Chinese Pharmacopoeia Commission, Pharmacopoeia of the People's Republic of China, 11th ed., China, 2020.
[37] M.C. Etter, Acc. Chem. Res. 23 (1990) 120–126.
[38] L.C. Wang, C.T. Seto, G.M. Whitesides, J. Am. Chem. Soc. 115 (1993) 905–916.
[39] M. Khan, V. Enkelmann, G. Brunklaus, Cryst. Growth Des. 9 (2009) 2354–2362.
[40] D.X. Li, M.M. Kong, J. Li, et al., CrystEngComm 20 (2018) 5112–5118.
[41] N.F. Frazão, E.L. Albuquerque, U.L. Fulco, et al., J. Nanosci. Nanotechnol. 16 (2016) 4825–4834.
[42] C.F. Mackenzie, P.R. Spackman, D. Jayatilaka, et al., IUCrJ 4 (2017) 575–587.
[43] N.K. Thakral, R.L. Zanon, R.C. Kelly, et al., J. Pharm. Sci. 107 (2018) 2969–2982.
[44] K. Korhammer, K. Neumann, O. Opel, et al., Appl. Energy 230 (2018) 1255–1278.
[45] R. Li, B.C. Dai, Y.D. Zhao, et al., Spectral Anal 29 (2009) 240–243.
[46] Z. Huang, S. Staufenbiel, R. Bodmeier, Pharm. Res. 39 (2022) 949–961.
[47] L.K. Mapp, S.J. Coles, S. Aitipamula, Cryst. Growth Des. 17 (2017) 163–174.
[48] X.L. Dai, J.M. Chen, T.B Lu, CrystEngComm 20 (2018) 5292–5316.
[49] L.N. Kuleshovaa, D.W.M. Hofmanna, R. Boese, Chem. Phys. Lett. 564 (2013) 26–32.
[50] M.L. Cheney, N. Shan, E.R. Healey, et al., Cryst. Growth Des. 10 (2010) 394–405.
[51] S.Z. Ren, M.Y. Liu, C. Hong, et al., Acta Pharm. Sin. B 9 (2019) 59–73.
[52] N.J. Babu, A. Nangia, Cryst. Growth Des. 11 (2011) 2662–2679.
[53] L.S. Reddy, S.J. Bethune, J.W. Kampf, et al., Cryst. Growth Des. 9 (2009) 378–385.
[54] Y.F. Wei, L. Zhang, N.N. Wang, et al., Cryst. Growth Des. 18 (2018) 7343–7355.